Available online at www.sciencedirect.com

SCIENCE DIRECT

Biochimica et Biophysica Acta 1716 (2005) 126 – 136

BIOCHIMICA ET BIOPHYSICA ACTA BBA

http://www.elsevier.com/locate/bba

# Membrane perturbation effects of peptides derived from the N-termini of unprocessed prion proteins

Mazin Magzoub [a], Kamila Oglęcka [a], Aladdin Pramanik [b], L.E. Göran Eriksson [a], Astrid Gräslund [a,*]

[a] *Department of Biochemistry and Biophysics, The Arrhenius Laboratories, Stockholm University, S-106 91 Stockholm, Sweden*
[b] *Department of Medical Biochemistry and Biophysics, Karolinska Institute, S-171 77 Stockholm, Sweden*

Received 17 June 2005; received in revised form 5 August 2005; accepted 2 September 2005
Available online 21 September 2005

**Abstract**

Peptides derived from the unprocessed N-termini of mouse and bovine prion proteins (mPrPp and bPrPp, respectively), comprising hydrophobic signal sequences followed by charged domains (KKRPKP), function as cell-penetrating peptides (CPPs) with live cells, concomitantly causing toxicity. Using steady-state fluorescence techniques, including calcein leakage and polarization of a membrane probe (diphenylhexatriene, DPH), as well as circular dichroism, we studied the membrane interactions of the peptides with large unilamellar phospholipid vesicles (LUVs), generally with a 30% negative surface charged density, comparing the effects with those of the CPP penetratin (pAntp) and the pore-forming peptide melittin. The prion peptides caused significant calcein leakage from LUVs concomitant with increased membrane ordering. Fluorescence correlation spectroscopy (FCS) studies of either rhodamine-entrapping (REVs) or rhodamine-labeled (RLVs) vesicles, showed that addition of the prion peptides resulted in significant release of rhodamine from the REVs without affecting the overall integrity of the RLVs. The membrane leakage effects due to the peptides had the following order of potency: melittin > mPrPp > bPrPp > pAntp. The membrane perturbation effects of the N-terminal prion peptides suggest that they form transient pores (similar to melittin) causing toxicity in parallel with their cellular trafficking.


*Keywords:* Prion protein; Phospholipid vesicle; Membrane perturbation; Fluorescence; FCS; CD

## 1. Introduction

Prion diseases, also known as transmissible spongiform encephalopathies, are fatal neurological disorders of humans and animals that appear in sporadic, familial and infectiously acquired forms. These disorders are caused by conversion of a normal neuronal glycoprotein ($PrP^C$) into an infectious, conformationally altered isoform ($PrP^{Sc}$) [1–3].

The conversion of $PrP^C$ into $PrP^{Sc}$ occurs via a post-translational process [4]. $PrP^C$ is monomeric and readily digested by proteinase K, whereas $PrP^{Sc}$ forms insoluble aggregates and shows a high resistance to proteolytic digestion [5]. The characteristics of the two forms of the prion protein (PrP) can be related to their differences in secondary structure. $PrP^C$ adopts a predominantly α-helical structure in its globular C-terminal half, and its N-terminus is largely unstructured [6], whereas $PrP^{Sc}$ has a large content of β-sheet secondary structure [7].

*Abbreviations:* PrP, prion protein; $PrP^C$, cellular isoform of PrP; $PrP^{Sc}$, scrapie isoform of PrP; mPrPp, peptide with sequence corresponding to the N-terminus of the mouse prion protein, residues 1–28; bPrPp, peptide with sequence corresponding to the N-terminus of the bovine prion protein, residues 1–30; NLS, nuclear localization sequence; CPP, cell-penetrating peptide; pAntp, penetratin, Antennapedia homeodomain-derived CPP; ER, endoplasmic reticulum; DHPC, 1,2-dihexanoyl-*sn*-glycero-3-phosphatidylcholine; POPC, 1-palmitoyl-2-oleoyl-*sn*-glycero-3-phosphocholine; POPG, 1-palmitoyl-2-oleoyl-*sn*-glycero-3-phosphoglycerol; POPG/POPC, [30/70] notation refers to vesicles with 30 mol% POPG content; SUVs, small unilamellar vesicles; LUVs, large unilamellar vesicles; Rh, rhodamine; REVs, Rh-entrapping LUVs; RLVs, Rh-labeled LUVs; FCS, fluorescence correlation spectroscopy; CD, circular dichroism; DPH, diphenylhexatriene, membrane bound fluorescence probe; P/L, total peptide-to-phospholipid molar ratio

* Corresponding author. Tel.: +46 8 162450; fax: +46 8 155597.
*E-mail address:* astrid@dbb.su.se (A. Gräslund).

0005-2736/$ - see front matter © 2005 Elsevier B.V. All rights reserved.
doi:10.1016/j.bbamem.2005.09.009

$PrP^C$ is unusual in that it can adopt multiple membrane topologies during biogenesis at the ER membrane [8–12]. Most $PrP^C$ molecules are fully translocated into the lumen of the ER; this form, denoted $^{Sec}PrP$, is eventually attached to the outer leaflet of the plasma membrane through a C-terminal glycosylphosphatidylinositol (GPI) anchor. Some $PrP^C$ molecules assume transmembrane orientations. These forms, designated $^{Ctm}PrP$ and $^{Ntm}PrP$, span the ER lipid bilayer once, either with the C- or N-terminus, respectively, on the lumenal side of the ER.

The signal sequence of $^{Sec}PrP$ is normally cleaved by a signal peptidase that acts in the lumen of the ER. However, in a recent study, it has been shown that in neuronal cells, the $^{Sec}PrP$ form retains its N-terminal signal sequence following its exit from the ER and during its trafficking to the cell surface [11]. It has also been reported that $^{Ctm}PrP$ is unprocessed and contains an uncleaved N-terminal signal peptide [13]. The signal sequence appears to have an unusual role in prion proteins in that it has two separate functions, both targeting and topogenesis [13–15]. It has also been suggested that $^{Ctm}PrP$ is associated with the neurodegeneration observed in prion disease [9]. Another variant of PrP discussed as a neurotoxic intermediate is cytosolic PrP, $^{Cyt}Pr$, which also sometimes retains the signal peptide [16–18]. Hence, even if the situations where unprocessed prion proteins appear may be relatively rare, these situations may be important for a pathological process.

Previously, we have investigated certain properties of the N-termini of the unprocessed mouse (residues 1–28) and bovine (residues 1–30) PrPs, denoted mPrPp [19] and bPrPp [20], respectively. These sequences (Table 1) comprise the signal peptide (residues 1–22 for mPrPp, residues 1–24 for bPrPp) and an identical and highly positively charged, NLS-like, sequence (residues 23–28 for mPrPp, residues 25–30 for bPrPp). The mPrPp and bPrPp sequences are similar to those of certain chimeric cell-penetrating peptides (CPPs), and we found that mPrPp and bPrPp can indeed function as CPPs ([21], and Magzoub et al., unpublished results). CPPs are able to translocate into various cells, carrying a conjugated hydrophilic macromolecular 'cargo' [21,22]. Recent observations on CPP entry into cells emphasize the role of heparan sulphate as a mediator of raft-dependent macropinocytosis, a particular form of endocytosis [23,24]. Cellular heparan sulphate has also been shown to interact with prion proteins [25], and $PrP^{Sc}$ incorporation into CHO cells requires glycosaminoglycan expression [26]. The interaction of various forms of PrP with model membranes have also been investigated [27,28].

In the present study, we have studied the interactions of mPrPp and bPrPp with large unilamellar phospholipids vesicles (LUVs) of varying surface charge densities, using fluorescence and CD spectroscopic methods. The membrane interaction effects of the two prion peptides were compared with those of two well-characterized peptides: the CPP penetratin (pAntp), and the pore-forming peptide melittin (Table 1). The steady-state fluorescence studies were complemented by fluorescence correlation spectroscopy (FCS) studies. FCS gives information on the translational diffusion of fluorescent particles with high specificity [29].

## 2. Materials and methods

### 2.1. Materials

The prion peptides and pAntp were produced by Neosystem Laboratoire, Strasbourg. Peptides were used as purchased. The identity and purity were controlled by amino acid, mass spectral and HPLC analyses. Peptides were of Immunograde quality (purity estimated at ~80%). In each case, peptides from more than one batch were used. Melittin from the venom of honeybee (*Apis mellifera*) was obtained from Sigma. 1-palmitoyl-2-oleoyl-phosphatidylcholine (POPC), and 1-palmitoyl-2-oleoyl-phosphatidylglycerol (POPG), were purchased from Avanti Polar Lipids, Alabaster, of the best quality, and were used without further purification. Diphenylhexatriene (DPH) was obtained from Sigma. Rh (tetramethylrhodamine-5,6-isothiocyanate) and Rh-PE (6-tetramethylrhodamine-1,2-dihexadecanoyl-3-phosphoethanolamine) were purchased from Molecular Probes, The Netherlands. Calcein, a fluorescein derivative, was also purchased from Molecular Probes (product no. C-481).

### 2.2. Determination of peptide concentrations

After weighing on a microbalance, the peptide concentrations in the stock solutions were determined by light absorption on a CARY 4 Spectrophotometer, using quartz cuvettes with a 1-cm light path. All spectra were baseline corrected. Molar absorptivities of 5690 and 1280 $M^{-1}$ $cm^{-1}$, at 280 nm, for tryptophan and tyrosine, respectively, were applied.

### 2.3. Sample preparations

#### 2.3.1. Preparation of LUVs

Large unilamellar vesicles were prepared by initially dissolving the phospholipids at the desired concentration (with the chosen POPG/POPC molar ratio) in a chloroform/ethanol mixture, to ensure complete mixing of the components, and then removing the solvent by placing the sample in a high vacuum for 3 h. The dried lipids were dispersed in 50 mM potassium phosphate buffer (pH 7.4). The dispersion was run through a freeze–thaw cycle five times and then passed through two polycarbonate filters (0.1 μm pore size) 20 times in an Avanti manual extruder.

#### 2.3.2. Preparation of REVs and RLVs

To prepare the Rh-entrapping LUVs (REVs), prior to extrusion, the dried lipid film (prepared as described above) was dispersed in 50 mM potassium

Table 1
The origin and amino acid sequences of the four peptides studied[a]

| Peptide | Origin | Sequence | Net charge | Hydrophobicity[b] |
|---|---|---|---|---|
| pAntp | Homeodomain (*Drosophila*) | RQIKIWFQNRRMKWKK | +7 | −1.7 |
| mPrPp | N-terminus of mouse prion protein (residues 1 to 28) | MANLGYWLLALFVTMWTDVGLC KKRPKP | +3 | 0.3 |
| bPrPp | N-terminus of bovine prion protein (residues 1 to 30) | MVKSKIGSWILVLFVAMWSDVGLCKKRPKP | +5 | 0.4 |
| Melittin | Honeybee venom (*Apis mellifera*) | GIGAVLKVLTTGLPALISWIKRKRQQ | +5 | 0.3 |

[a] Given are also the net charges of the peptides, as well as their average hydrophobicities. The charged residues are underlined.
[b] The average hydrophobicity of the peptides is calculated using the scale devised by Kyte and Doolittle [60].

phosphate buffer containing 200 nM Rh. In this case, the LUVs entrapped the dissolved Rh, which can be released if pore/channels are formed into the vesicles, or if the vesicles are broken. A Rh concentration gradient was created by diluting the REV samples 100- to 200-fold in the buffer, resulting in a less than 1 nM background Rh concentration outside the vesicles.

To prepare the Rh-labeled LUVs (RLVs), the phospholipids, including 0.1 mol% Rh-labeled lipids, were dissolved in the chloroform/ethanol mixture prior to making the lipid film. Rh is covalently bound to the head-groups of the phosphatidylethanolamine, and only the disintegration of the RLVs can lead to the appearance of faster diffusing Rh in solution.

### 2.4. Steady-state fluorescence spectroscopy

Fluorescence was measured on a Perkin Elmer LS 50B Luminescence Spectrometer with FL WinLab software. Measurements were made in $4 \times 10$ mm quartz cuvettes at 20 °C. For DPH experiments the excitation was at 340 nm and the emission wavelength scanned from 400 to 550 nm. Calcein was excited at 490 nm and the emission scanned from 510 to 600 nm. Scans were usually recorded with 4 nm excitation and emission bandwidths and a scan speed of 250 nm/min. 3 scans were recorded and averaged for each sample.

#### 2.4.1. Peptide-induced calcein release

LUVs with entrapped calcein were prepared by hydrating a lipid film of desired composition with 70 mM calcein present in the buffer (the final pH was adjusted to 7.4 by the addition of NaOH from a 10-M stock solution). The fluorescence from calcein at 70 mM was low due to self-quenching, but increased considerably upon dilution. Free calcein was separated from the LUVs on a Sephadex-G25 column. Increasing concentrations of peptides were added (from a 1-mM stock solution) to LUVs composed of 250 μM phospholipid mixtures of different POPG/POPC content. After 5-min incubation, release of calcein from the LUVs was monitored by an increase in the fluorescence intensity.

The maximum fluorescence intensity corresponding to 100% leakage was determined by lysing the vesicles with 10% (w/v) Triton X-100. The % leakage was then calculated according to the following equation:

$$\%\ \text{leakage} = 100\left(\frac{F - F_0}{F_{\max} - F_0}\right) \tag{1}$$

where $F_0$ represents the fluorescence intensity of the intact vesicles, $F$ and $F_{\max}$ the intensity before and after the addition of the detergent, respectively.

#### 2.4.2. Fluorescence polarization

LUVs were labeled with the membrane-bound probe diphenylhexatriene (DPH). 2 μM DPH (from a 1 mM ethanolic stock solution) was added to LUVs composed of 200 μM phospholipid mixtures of different POPG/POPC content. The samples were allowed to equilibrate for 15 min before measurement. Increasing concentrations of peptides, from a 1-mM stock solution, were added to the labeled LUV samples, and allowed to stand for 10 min. A polarization attachment (Shimadzu) was adapted to the spectrometer. The steady-state polarization was determined using the following equation [30]:

$$P = \frac{I_{VV} - GI_{VH}}{I_{VV} + GI_{VH}} \tag{2}$$

where $I_{VV}$ is the emission intensity of vertically polarized light parallel to the plane of excitation and $I_{VH}$ is the emission intensity of horizontally polarized light perpendicular to the plane of excitation. The instrumental factor $G$ ($G = I_{HV}/I_{HH}$) was determined by measuring the polarized components of fluorescence of the probe with horizontally polarized excitation.

### 2.5. Fluorescence correlation spectroscopy (FCS)

#### 2.5.1. FCS instrumentation

FCS was performed with confocal illumination of a volume element of 0.2 fl in an instrument as described previously [31,32]. As focusing optics a Zeiss Neofluar $63 \times$ NA 1.2 was used in an epi-illumination setup. For separating exciting from emitted radiation a dichroic filter (Omega 540 DRL PO2) and a bandpass filter (Omega 565 DR 50) were used. REVs or RLVs were excited with the 514.5-nm line of an Argon laser. The fluorescence intensity fluctuations were detected by an avalanche photo diode (EG and SPCM 200) and were correlated with a digital correlator (ALV 5000, ALV, Langen, Germany).

#### 2.5.2. FCS data evaluation

The observed fluorescence intensity fluctuations $\delta I(t)$ when correlated with fluorescence intensity fluctuations at time $t+\tau$ yield the normalized intensity autocorrelation function $G(\tau)$:

$$G(\tau) = 1 + \frac{\langle \delta I(t)\tau I(t+\tau)\rangle}{\langle I\rangle^2} \tag{3}$$

where the brackets describe the time average and $I$ the mean fluorescence intensity [33,34].

The intensity autocorrelation function $G(\tau)$ for Brownian motion of molecules/particles in a 3D Gaussian volume element is described [35] as follows:

$$G(\tau) = 1 + \frac{1}{N}\left(\frac{1}{1+\frac{4D\tau}{\omega^2}}\right)\left(\frac{1}{1+\frac{4D\tau}{z^2}}\right)^{\frac{1}{2}}$$

$$\text{or } G(\tau) = 1 + \frac{1}{N}\left(\frac{1}{1+\frac{\tau}{\tau_D}}\right)\left(\frac{1}{1+\left(\frac{\omega}{z}\right)^2\frac{\tau}{\tau_D}}\right)^{\frac{1}{2}} \tag{4a}$$

where $\tau_D$ is the characteristic translational diffusion time related to the diffusion

$$\text{coefficient } D: \tau_D = \frac{\omega^2}{4D} \tag{4b}$$

and $N$ is the total number of detected fluorescence molecules, $\omega$ (0.5 μm) is the radius, and z (2 μm) the length of the volume element of the laser beam.

The expressions for the intensity autocorrelation function $G(\tau)$ (Eqs. (3) (4a) (4b)) are valid when the particle size is smaller than the volume element. With a volume element of a diameter of 1 μm and a vesicle size of 0.1 μm this condition is fulfilled. To calculate the average number of fluorophores per volume element ($N$), and diffusion coefficients of free Rh ($D_F$) and labeled vesicles ($D_V$), the intensity autocorrelation function $G(\tau)$ is analyzed as follows:

$$G(\tau) = 1 + \frac{1}{N}\left[(1-y)\left(\frac{1}{1+\frac{\tau}{\tau_{D_F}}}\right)\left(\frac{1}{1+\left(\frac{\omega}{z}\right)^2\frac{\tau}{\tau_{D_F}}}\right)^{\frac{1}{2}} + y\left(\frac{1}{1+\frac{\tau}{\tau_{D_V}}}\right)\left(\frac{1}{1+\left(\frac{\omega}{z}\right)^2\frac{\tau}{\tau_{D_V}}}\right)^{\frac{1}{2}}\right] \tag{5}$$

where $N$ is the total number of fluorophores, $\tau_{Dv} = \omega^2/4D_v$ is the diffusion time for vesicles, $\tau_{DF} = \omega^2/4D_F$ is the diffusion time for free Rh, $y$ is the fraction of Rh diffusing with the vesicles having the characteristic diffusion time $\tau_{Dv}$, and $(1-y)$ is the fraction of free Rh diffusing with $\tau_{DF}$. For parametrization and fitting of the autocorrelation function $G(\tau)$, a non-linear least squares minimization procedure according to the Marquardt algorithm [36] was used.

#### 2.5.3. FCS experiments

Free Rh was used as a reference to calibrate the instrument and to estimate diffusion times of the RLVs, as well as to observe whether the vesicles are intact or destroyed. The diffusion times of free Rh and RLVs were determined separately. The effect of the peptides on vesicles was investigated by incubating the vesicles together with the peptides. The total peptide-to-phospholipid molar ratio (P/L) ratio varied from 0.05 to 0.1. 20 μl of the samples were analyzed for 30 s up to 10 min in the FCS instrument, at several time points of incubation, ranging from minutes to hours. All experiments were performed at 20 °C.

### 2.6. Circular dichroism spectroscopy (CD)

CD measurements were made on a Jasco J-720 CD spectropolarimeter with 0.5 and 1 mm quartz cuvettes. Spectra were measured from 190 to 250 nm, with a 0.2-nm step resolution at 50 nm/min speed. The response time was 2 s,

with 50 mdeg sensitivity and a 1-nm bandwidth. The temperature was regulated by a PTC-343 controller, set at 20 °C. Spectra were collected and averaged over 20 scans. Contributions from background signals were subtracted from the CD spectra acquired for the peptide. Computer fittings using the VARSELEC program [37], with 3 reference component spectra (α-helix, β-sheet and random coil, r.c.) were performed to estimate the contributions of spectral components from different secondary structures. The percentages describing the contributions are precise within 5–10%.

## 3. Results

Table 1 shows the sequences of the mouse and bovine prion peptides (mPrPp and bPrPp, respectively), as well as the two archetypal peptides (pAntp and melittin). The pAntp sequence corresponds to the 16 residues of the third α-helix of the Antennapedia homeodomain protein from *Drosophila* and is a well-known CPP [21]. Melittin is a 26-residue peptide derived from honeybee venom, and is a well-known pore-forming peptide [38].

### 3.1. Peptide-induced calcein release from LUVs

The membrane-perturbing effects of the peptides were investigated through calcein-release experiments in LUVs. The calcein-release assay is based on a high concentration (up to 70 mM) of entrapped calcein, resulting in self-quenching of its fluorescence. The degree of leakage of the vesicles induced by the peptides is assessed by observing increased fluorescence from the released calcein.

Fig. 1a shows the % leakage induced by the peptides with neutral POPC LUVs, after 5 min exposure, at 20 °C. A study of the time-dependence of calcein leakage from LUVs (Fig. 1b, inset) indicated that the process is a relaxation towards an equilibrium, and has a duration of approximately 5 min, after which no further leakage takes place. Thus, the levels of leakage presented in Fig. 1 should represent the final stage at each peptide concentration. The results are summarized in Table 2.

pAntp, which does not interact with neutral membranes [39,40], induced no leakage. Addition of bPrPp or mPrPp to the neutral LUVs results in substantial degrees of leakage, 40% and 66%, respectively. The leakage by the prion peptides occurs at low peptide concentrations, where maximum leakage is achieved at P/L ~0.1, corresponding to 25 μM peptide. Melittin was found to be far more potent: approximately 100% leakage was induced already at P/L ~0.02.

The leakage from charged POPG/POPC [30/70] LUVs induced by the peptides is shown in Fig. 1b (results are summarized in Table 2). Although pAntp does interact with the charged vesicles [40], there is relatively little leakage effect. bPrPp and mPrPp cause higher degrees of leakage, 54% and 74%, respectively, which are higher degrees of leakage than with the neutral LUVs. Melittin gives 100% leakage, at a somewhat higher P/L ~003, as compared with the POPC LUVs.

### 3.2. DPH fluorescence polarization

The perturbation effects of the peptides on the membrane properties of LUVs were studied by steady-state fluorescence

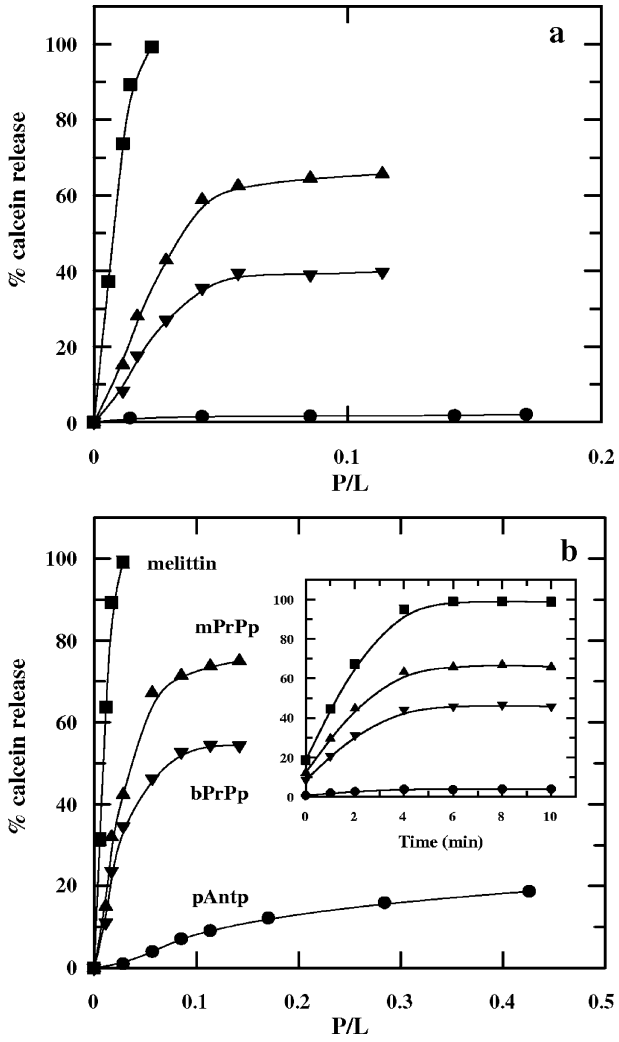


Fig. 1. Calcein leakage from LUVs, induced by the peptides: mPrPp (▲), bPrPp (▼), pAntp (●) and melittin (■). Increasing concentrations of the peptides were added to LUV samples, composed of 250 μM phospholipid of different POPG/POPC content. The LUVs had 70 mM calcein entrapped in the beginning. The samples contained (a) POPC or (b) POPG/POPC [30/70]. The % calcein release was plotted as a function of total peptide-to-lipid molar ratio, P/L. The medium was 50 mM phosphate buffer (pH 7.4). The spectra were recorded at an ambient temperature (20 °C). Inset: time-dependence of calcein leakage due to addition of peptides at P/L=0.05.

polarization of the DPH probe. When added to a membrane suspension, DPH dissolves completely into the bilayer core, with no significant emission in the aqueous phase. Since DPH is buried deeply within the acyl chain region of the bilayer, any increase in polarization reports on decreased acyl chain mobility [41,42].

Fig. 2a shows the effect of addition of the peptides to neutral POPC LUVs on the DPH polarization. Due to lack of binding [39], pAntp does not significantly affect the DPH polarization of the neutral vesicles. mPrPp and bPrPp, which are hydrophobic enough to bind to neutral membranes, increase the DPH polarization, with mPrPp inducing a greater increase in membrane ordering than bPrPp. Melittin, causes a slight decrease in the polarization, indicating that melittin decreases the membrane ordering, leading to greater fluidity

Table 2
Summary of membrane activities and secondary structures of the peptides[a]

| Peptide | Medium | Secondary structure component (%) (P/L=0.04) | | | Polarization Δ(P) (P/L=0.1) | % calcein release (P/L=0.1) |
|---|---|---|---|---|---|---|
| | | α | β | r.c. | | |
| pAntp | Water | 13 | 24 | 62 | – | – |
| | Buffer | 14 | 25 | 60 | – | – |
| | POPC | 14 | 22 | 63 | 0 | 2 |
| | [30/70] | 33 | 24 | 42 | 0 | 9 |
| | POPG | 19 | 48 | 33 | 0.05 | 50 |
| bPrPp | Water | 15 | 25 | 59 | – | – |
| | Buffer | 25 | 34 | 41 | – | – |
| | POPC | 28 | 39 | 31 | 0.01 | 40 |
| | [30/70] | 11 | 55 | 32 | 0.06 | 54 |
| mPrPp | Water | 18 | 26 | 56 | – | – |
| | Buffer | 24 | 32 | 44 | – | – |
| | POPC | 30 | 36 | 33 | 0.03 | 66 |
| | [30/70] | 15 | 51 | 34 | 0.07 | 74 |
| Melittin | Water | 16 | 15 | 67 | – | – |
| | Buffer | 28 | 11 | 60 | – | – |
| | POPC | 58 | 22 | 20 | −0.02 | 100 |
| | [30/70] | 60 | 24 | 16 | 0.05 | 100 |

[a] Given are the changes in polarization (ΔP) and the % calcein release in the presence of LUVs with different compositions, at P/L ~0.1. Also included are the secondary structures induced in the peptides in the presence of distilled water and 50 mM phosphate buffer, pH 7.4, as well as the LUVs under conditions where the two prion peptides are fully bound.

within the acyl-chain region of the bilayer. The result is in agreement with a published study in which melittin was found to induce lipid flip-flop in neutral, but not charged, LUVs [43].

The effect of the peptides on charged LUVs from POPG/POPC [30/70] is shown in Fig. 2b. pAntp induces no significant change in the DPH fluorescence polarization. This is probably due to the location of pAntp at the membrane surface, within the headgroup region [40,44]. The prion peptides cause a considerable increase in the DPH polarization, with mPrPp inducing a slightly higher increase than bPrPp. The interaction of melittin with the charged LUVs, unlike with the neutral ones, resulted in a small increase in the DPH polarization.

Table 2 includes estimated changes (+/−) in the DPH polarization ($\Delta P$) values induced by the four peptides at an arbitrary P/L=0.1, with POPC and POPC/POPG [30/70] LUVs. The leakage effects for mPrPp, bPrPp and pAntp mirror their polarization influences: an increased LUV surface charge density results in a greater degree of polarization and a higher degree of leakage induced by the peptides. The effects are more pronounced for melittin, followed by the prion peptides.

### 3.3. FCS

In FCS measurements, the fluorescence intensity fluctuations are recorded only from the molecules that diffuse through the confocal laser volume element. The time required for the passage of molecules through the volume element is determined by the diffusion coefficient, related to the size and shape of molecules. From the autocorrelation functions of fluorescence intensity fluctuations, the average number ($N$) and the diffusion time ($\tau_D$) of fluorescent molecules or particles crossing the confocal volume are determined.

#### 3.3.1. FCS parameters

Fluorescence intensity autocorrelation functions, $G(\tau)$, of free Rh, POPG/POPC [30/70] REVs and RLVs (i.e. LUVs with 30% POPG content) are shown in Fig. 3a–c, respectively. In the REV preparation, the Rh concentrations inside and outside the vesicles were 200 nM and 2 nM, respectively. Table 3 summarizes the evaluated values of $\tau_D$ in each case. A two-component analysis of the autocorrelation curves was used to yield a slowly diffusing bound component (Rh diffusing with the LUVs) and a fast moving non-bound one (freely diffusing Rh). The diffusion time of free Rh in solution is 0.070±0.002 ms. The major component of the diffusion time of the REVs (where the entrapped Rh diffuses with the vesicles) is 7.4±1 ms; a minor component (15%) has the $\tau_D$ of free Rh (interpreted as the contribution from the free fraction of Rh).

The $\tau_D$ calculated for the RLVs id 8.4±1 ms. Due to the large difference in diffusion times between free Rh and vesicles, the fractions of Rh free in solution and diffusing with the vesicles (either entrapped or covalently-bound), can be seen separately and comparative observations can be made. However, absolute quantifications of Rh release are not reliable due to the large difference in fluorescence intensities between Rh-entrapping vesicles and free Rh—the so-called 'brightness ratio'—which distorts the quantification (cf. [45]). In addition, the tendency of Rh to bind to the surface of vesicles (Rh+LUVs, Table 3) further contributes to the uncertainty concerning the precise quantification of release of entrapped Rh.

#### 3.3.2. Effect of peptides on RLVs

Addition of melittin to POPG/POPC [30/70] RLVs, at P/L=0.05, and mPrPp, bPrPp or pAntp at P/L=0.1, results in no change in the RLV diffusion time (8.4±1 ms, Table 3), showing that there is no free Rh in solution and that the LUVs are intact. At the chosen P/L (0.1) for these studies both mPrPp

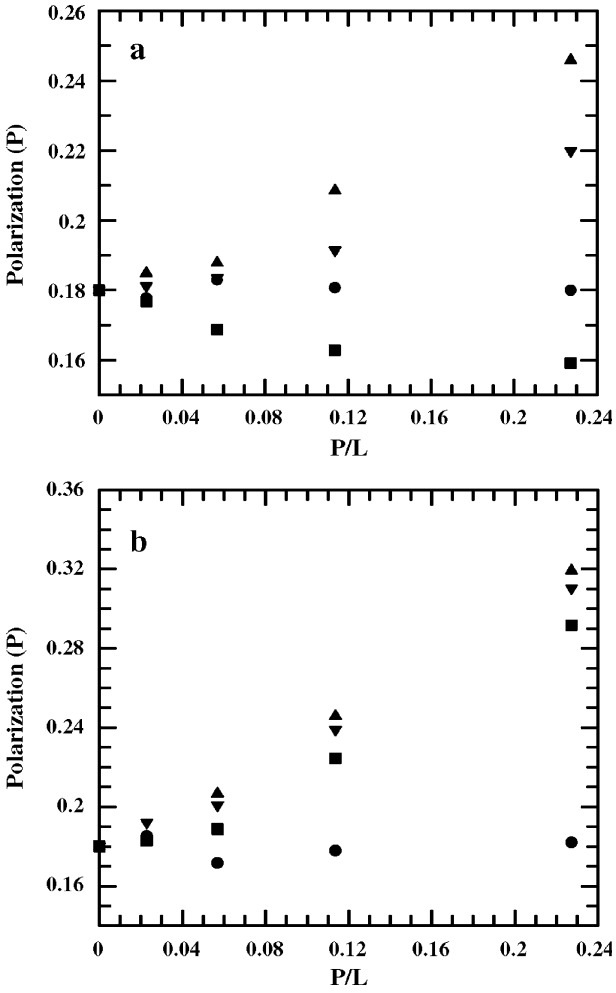


Fig. 2. Change in the fluorescence polarization of DPH labeled LUVs upon addition of the peptides: mPrPp (▲), bPrPp (▼), pAntp (●) and melittin (■). The LUVs were composed of 250 μM phospholipid samples of different POPG/POPC content, and containing 2 μM DPH. The LUV samples contained (a) POPC or (b) POPG/POPC [30/70]. The polarization was plotted as a function of P/L. 50 mM phosphate buffer medium (pH 7.4) was used. The spectra were recorded at an ambient temperature.

and bPrPp are still in a fully bound state, as observed by changes in fluorescence intensity of the intrinsic tryptophan due to addition of vesicles (data not shown). This particular P/L was also chosen since it allows a near maximum effect of these peptides on the vesicles to be observed, while avoiding artifacts such as LUV aggregation (data not shown).

### 3.3.3. Peptide-induced Rh release from REVs

FCS was used to monitor the release of entrapped Rh (200 nM) from REVs due to the peptides. Upon the addition of melittin to the REVs (Fig. 3d), at a total peptide-to-phospholipid molar ratio (P/L)=0.05, the evaluated fraction of free Rh increases from 15% to approx. 80% (Table 3), indicating that addition of melittin results in release of Rh from the REVs, in agreement with previous studies [46,47].

Addition of the two prion peptides, mPrPp and bPrPp (Fig. 3e and f, respectively), at P/L=0.10, results in an increase in the total fraction of free Rh to 70% and 65%, respectively (Table 3), illustrating also for these peptides the release of Rh from the REVs. Exposure of the REVs to pAntp (P/L=0.1) results in a small increase in the total free fraction to ~20%, indicating a weak effect of the peptide, possibly due to release of peptide associated with the outside of the vesicle (Table 3).

Values of the number of diffusing particles $N$ are included in Table 3. The value of $N$ increases from ~0.3 for REVs alone to ~2.8 upon addition of melittin, indicating an increase in the number of fluorophores in solution. With the prion peptides the value of $N$ again increases, but to a lesser extent than with melittin ($N$ ~1.3 and 1.1 for mPrPp and bPrPp, respectively). No change in the value of $N$ is observed upon addition of pAntp. This confirms the increase in apparent fraction of free Rh upon addition of melittin and the prion peptides to the REVs inferred from the $\tau_D$ observations.

Lysing the LUVs with Triton X-100 (10% w/v) results in a ~65% fraction of freely diffusing Rh, with $\tau_D$ ~0.07 ms (data not shown). The remainder has a $\tau_D$ of 0.5 ms, indicating complex formation between Rh and phospholipids (micelles). Incubation of non-labeled LUVs with free Rh results in a fraction of the Rh (~30%) diffusing with the LUVs ($\tau_D$=7.4 ms), while the value of $N$ decreases from 3.2 to 2.4, which confirms the affinity of Rh for lipids (Table 3). Taken together, the FCS results with melittin and the prion peptides indicate that under conditions where leakage of vesicle content is observed, the overall integrity of the vesicle is intact.

### 3.4. Peptide secondary structures

The secondary structures induced in the peptides in the presence of water, buffer and LUVs of different lipid compositions, were studied by CD spectroscopy (Fig. 4). In all experiments the peptide concentration was 4 μM, and the phospholipid concentration was 100 μ (P/L=0.04). Under these conditions, the prion peptides were found to be in the fully membrane bound state, verified by fluorescence experiments (data not shown). Table 2 summarizes the secondary structure contributions of the peptides evaluated for the various solvents. Although structure analysis of peptides by CD is at best approximate, significant trends are seen. In distilled water, all the peptides are largely in random coil secondary structure (data not shown). The presence of buffer ions (Fig. 4a) induces a somewhat higher degree of secondary structure in melittin (α-helix), mPrPp and bPrPp (β-sheet), but not in pAntp.

In the presence of neutral LUVs (Fig. 4b), the peptides, except for pAntp, become more structured. With its low hydrophobicity (Table 1), pAntp has a low binding affinity to an electrically neutral membrane [39,48], and hence remains unstructured. Introduction of charges (30%) to the LUV surface induces some α-helical structure in pAntp, whereas mPrPp and bPrPp increase their β-structure contributions to some extent (Fig. 4c; Table 2). Melittin, on the other hand, maintains the same high degree of helicity (Fig. 4c).

### 3.5. Vesicle aggregation due to pAntp

In the presence of partially charged vesicles, pAntp adopts a helical structure, and is generally ‘benign’, with

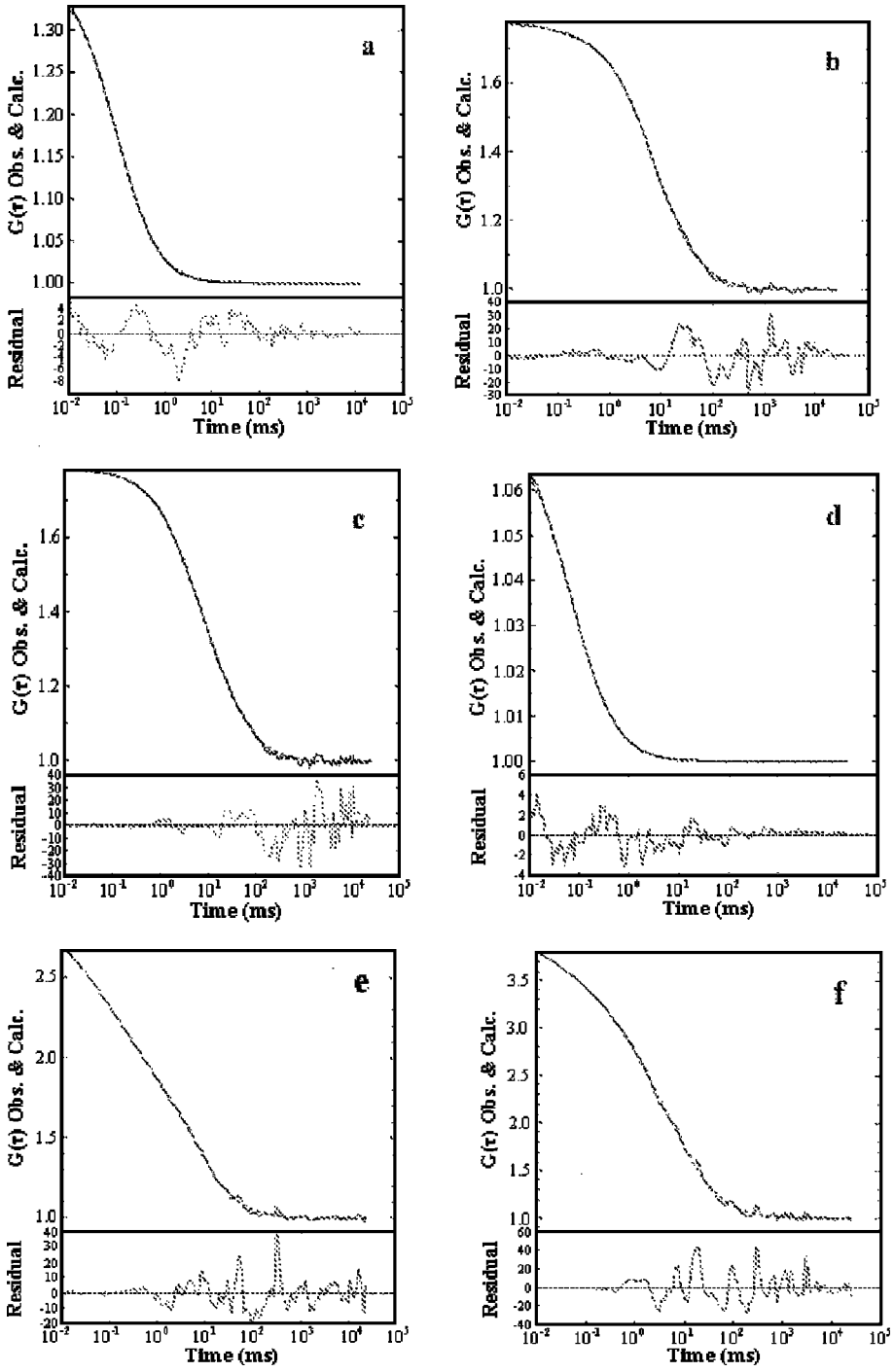


Fig. 3. The fluorescence intensity autocorrelation functions, $G(\tau)$, of: (a) free rhodamine (Rh) in solution; (b) rhodamine-entrapping LUVS (REVs); and (c) rhodamine-labeled LUVs (RLVs). The composition of the REVs and RLVs was POPG/POPC [30/70], with a total lipid concentration of 100 μM. The effect of the peptides on the REVs, following incubation period of 1 hr: fluorescence intensity autocorrelation function $G(\tau)$ of 100 μM REVs in the presence of : (d) 5 μM melittin (P/L=0.05); (e) 10 μM mPrPp (P/L=0.1); and (f) 10 μM bPrPp (P/L=0.1). The FCS parameters derived by fittings of the autocorrelation curves are summarized in Table 3. The medium in all cases was 50 mM phosphate buffer (pH 7.4), and all spectra were recorded at an ambient temperature (20 °C).

negligible membrane perturbation effects. However, we have previously observed that in the presence of fully charged vesicles, the peptide adopts a dominating β-structure, particularly at high P/L, and has pronounced membrane perturbation effects [40,48]. Here we use FCS, in tandem with steady-state fluorescence techniques, to characterize the interaction of pAntp with the fully charged POPG LUVs, in comparison with the partially charged POPG/POPC [30/70] vesicles.

Fig. 5a shows evaluated diffusion times, $\tau_D$, as a function of P/L for the RLVs with the two surface charges. A large increase in the RLV diffusion time for fully charged POPG vesicles is observed in the presence of pAntp, even at low peptide concentrations. This indicates a severe case of vesicle

Table 3
Summary of the FCS parameters derived from the intensity autocorrelation functions $G(\tau)$ of rhodamine (Rh)[a]

| Sample | | Bound/entrapped Rh fraction | | Free Rh fraction | | $N$ |
|---|---|---|---|---|---|---|
| | | $\tau_D$ (ms) | % | $\tau_D$ (ms) | % | |
| Rh | only | – | – | 0.07 | 100 | 3.2 |
| | +LUVs | 7.4 | 30 | 0.07 | 70 | 2.4 |
| RLVs | only | 8.4 | 100 | – | – | 0.4 |
| | +melittin | 8.4 | 98 | 0.07 | 2 | 0.5 |
| | +mPrPp | 8.4 | 98 | 0.07 | 2 | 0.5 |
| | +bPrPp | 8.4 | 99 | 0.07 | 1 | 0.4 |
| | +pAntp | 8.4 | 99 | 0.07 | 1 | 0.4 |
| REVs | only | 7.4 | 85 | 0.07 | 15 | 0.3 |
| | +melittin | 7.4[b] | 20 | 0.07 | 80 | 2.8 |
| | +mPrPp | 7.4[b] | 30 | 0.07 | 70 | 1.3 |
| | +bPrPp | 7.4[b] | 35 | 0.07 | 65 | 1.1 |
| | +pAntp | 7.4[b] | 80 | 0.07 | 20 | 0.3 |

[a] Given are the % fractions of Rh diffusing with the vesicles (entrapped in POPG/POPC [30/70] REVs or covalently bound to POPG/POPC [30/70] RLVs) or freely diffusing (non-bound) in the absence, or presence, of the peptides. The rhodamine (Rh) concentration in solution was 200 nM. The vesicles (with a phospholipid concentration of 100 μM for both REV and RLV samples) and the peptides (at a concentration of 10 μM, i.e. P/L=0.1, except for melittin, which was at 5 μM, P/L=0.05) were incubated for a period of 1 h. The fraction (%) of Rh diffusing with a certain $\tau_D$ was calculated using a two-component fitting of the autocorrelation curves.

[b] The $\tau_D$ for this component was fixed during the fitting procedure.

aggregation. In contrast, with POPG/POPC [30/70] RLVs, a small increase in $\tau_D$ was observed, and then only at the higher peptide concentrations (P/L>0.1). Thus, under the conditions of the experiments carried out with POPC and POPC/POPG [30/70] LUVs in this study, vesicle aggregation does not occur. LUV aggregation was also observed with POPG RLVs in the presence of the prion peptides, and aggregation comparable to that induced by pAntp was observed at the higher P/L values (Fig. 5a).

Fig. 5b shows the FCS kinetics of the aggregation of POPG RLVs in the presence of pAntp (P/L=0.05 and 0.1). With P/L=0.05 only a partial aggregation is observed. The aggregation process is completed within 5 min. Once aggregation takes place, the aggregates are stable up to 24 h (Fig. 5b inset), contrary to what has previously been reported from light scattering studies, where gradual disaggregation was observed, over a period of 1–2 h [49]. The higher degree of β-structure induced in pAntp with the POPG LUVs than with the POPG/POPC [30/70] LUVs (Table 2) was highly stable. We did not detect any transient secondary structure conversion back to α-helix under the present conditions.

Similar extreme properties of POPG LUVs with pAntp is observed with steady-state fluorescence: a significant increase in DPH polarization, and an increase in the calcein leakage (Table 2). The total fraction of free Rh increases to 60% upon addition of pAntp to POPG REVs (FCS data not shown).

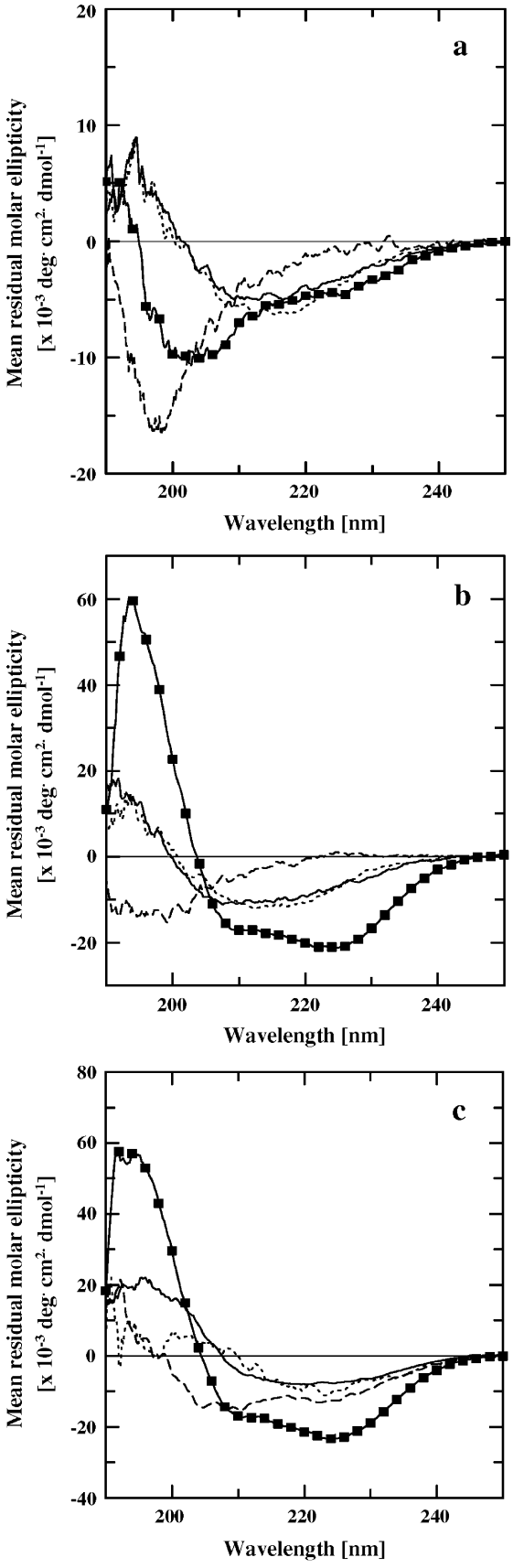


Fig. 4. CD Spectra of 4 μM of mPrPp (—), bPrPp (- - -), pAntp (– –) and melittin (–■–) in different media: (a) 50 mM phosphate buffer, and LUVs composed of (b) 100 μM POPC, or (c) 100 μM POPG/POPC [30/70]. The medium for the LUVs was 50 mM phosphate buffer (pH 7.4). The temperature was set at 20 °C.

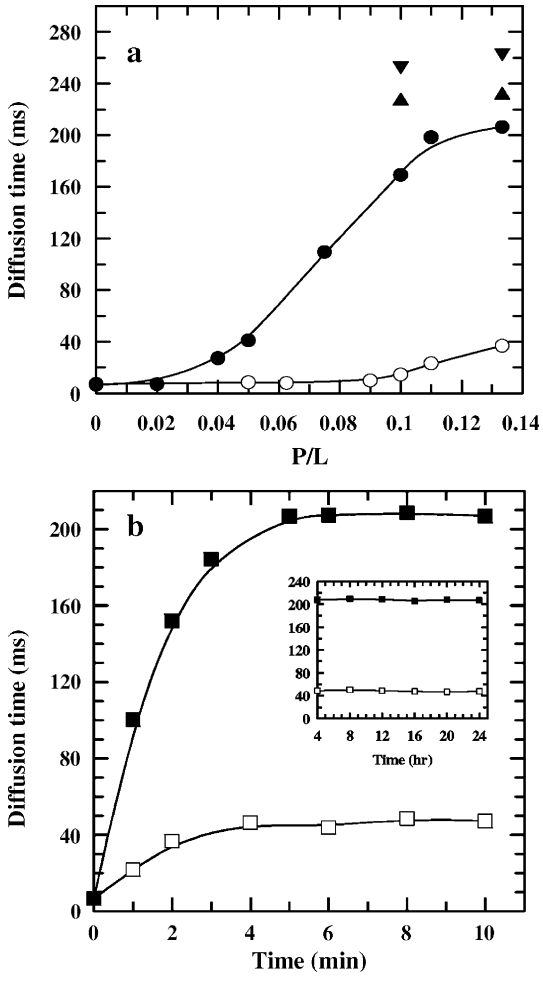


Fig. 5. LUV aggregation due to the peptides as determined by the diffusion times obtained by FCS. (a) pAntp induced aggregation of POPG/POPC [30/70] RLVs (○) and POPG RLVs (●). Also shown is the aggregation of POPG RLVs due to mPrPp (▲) and bPrPp (▼). Increasing concentrations of the peptides were added to the RLV samples, at a 100-μM phospholipid concentration, and containing 0.1 mol% Rh-labeled lipids. The diffusion time of the RLVs was plotted as a function of P/L. (b) Time-dependence of pAntp induced PG RLV aggregation, at P/L=0.10 (■) and P/L=0.05 (□). Inset: longer time-scale of the same measurement. The medium was 50 mM phosphate buffer (pH 7.4). The spectra were recorded at an ambient temperature (20 °C).

Taken together, these results suggest that vesicle aggregation and leakage are related for pAntp, where a high membrane surface charge promotes a large surface occupancy and concomitant β-structure promotion in the peptide.

## 4. Discussion

The present study focuses on the N-terminal signal peptide with an additional short basic domain of mouse and bovine unprocessed PrPs. The two prion peptides, mPrPp [21] and bPrPp (Magzoub et al., unpublished results), were previously found to function as cell-penetrating peptides (CPPs). In general, the low cytotoxic effects of typical CPPs, such as pAntp and the HIV-1 Tat peptide, distinguish them from translocating cationic antimicrobial and pore-forming peptides, such as melittin, which exhibit strong effects on the membrane integrity. However, like certain CPPs, particularly the amphipathic chimeras [22,23], the prion peptides produced membrane perturbations in cells, resulting in morphological stress [20], as well as hemolysis of red blood cells and leakage from CHO and neuronal N2A cells (Magzoub et al., unpublished results).

We have now studied the membrane perturbation effects of the prion-derived peptides in vesicle model systems, comparing the results with those of the archetypal CPP pAntp, and the pore-forming melittin. pAntp does not perturb the LUVs to any great extent (Figs. 1 and 2; Tables 2 and 3). Melittin, on the other hand, causes pronounced membrane disturbances. The peptide induces maximal leakage of entrapped calcein, and causes considerable release of Rh from the REVs (Figs. 1 and 3; Tables 2 and 3). Leakage from the LUVs can be caused either by completely destroying the vesicles (lysis) or by making channels into them (pore-formation). As the translational properties of the RLVs remain constant in the presence of melittin, under conditions where leakage from the REVs was observed in terms of P/L (Table 3), and an increase in membrane ordering is observed (Fig. 2), we conclude that pore-formation rather than lysis is the explanation for the observed effects. This agrees with numerous literature reports on melittin [38,46,47,50].

The two prion peptides, mPrPp and bPrPp, behave similarly to melittin, giving rise to substantial leakage of the vesicle contents (Figs. 1 and 3; Tables 2 and 3). The overall integrity of the vesicles is not affected, as indicated by the unchanged diffusion times of the RLVs (Table 3). This again suggests pore-formation caused by mPrPp and bPrPp. It is worth noting here that there is at present no consensus on the definition of the 'pore'. While some reports use the term to describe a defined structure, composed of a number of helices in a parallel alignment, others use it to describe a peptide-induced structural defect in the membrane through which ions or molecules can pass [38,51]. In the present context, we use the latter, broader definition. The orientation of melittin in lipid bilayers is dependent on a number of parameters, including P/L and lipid type. At the relatively high concentrations used here it is likely that melittin adopts a transmembrane orientation [52]. In an NMR study of bPrPp associated with neutral DHPC micelles [20], the results indicated that the induced α-helical structure observed under those conditions should have a transmembrane orientation, a positioning favouring pore-formation.

The kinetics of peptide-induced calcein leakage exhibits saturation (Fig. 1b). Such phenomena have been observed in several other studies of peptides interacting with membranes, yielding leakage curves which reach a plateau as a function of time at a constant peptide concentration [53–55]. The observations have been interpreted in terms of transient pore formation, involving a nucleation step during an initial bilayer perturbation period, followed by a transient restabilization of the peptide/lipid bilayer structure, which gives rise to the observed leveling off of the spontaneous leakage [56]. The saturation of the leakage curves for mPrPp and bPrPp as a function of peptide concentration (Fig. 1) may have a similar background. Alternatively, this behavior could be due to increased self-aggregation of the prion peptides taking place

at the higher peptide concentrations (Magzoub et al., unpublished results) resulting in attenuation of peptide activity.

The two prion peptides differ from melittin in that a higher membrane surface charge density leads to a greater effect on the membrane integrity. At the higher LUV surface charge density the peptides, with higher β-structure content (possibly in an aggregated state), have a more potent effect on the membrane integrity than observed with neutral membranes. This suggests that peptide aggregation and concomitant β-structure induction may be one prerequisite for pore-formation caused by the prion peptides.

When interacting with fully charged LUVs, pAntp adopts a β-structure [48] and causes vesicle aggregation and leakage (Fig. 5; Table 2). The high charge density of the fully charged LUVs promotes extreme behavior in both the vesicles and the peptides. The high surface charge density may lead to peptide aggregation (manifesting itself as β-structure), which in turn leads to vesicle aggregation. This could explain the increase in membrane DPH polarization observed here with fully charged LUVs (Table 2), as well as the previously reported large increase in the DPH polarization with the fully charged SUVs induced by pAntp [40]. The β-structure and vesicle aggregation are not completely interdependent, since we observe some β-structure even when there is no obvious vesicle aggregation (data not shown).

In this study, we have attempted to complement the traditional calcein release assay with a more novel release assay using FCS. Although the parameters measured in both cases are different—fluorescence 'de-quenching' as opposed to translational diffusion—while the concentration gradients involved are also rather different, the two methods obviously give similar and complementary results.

Calcein-release is an established method. Self-quenching of calcein has been attributed to a combination of dimerization and energy transfer [57]. However, the high concentrations of the entrapped calcein used (~55–70 mM) is problematic. For instance, at higher prion peptide concentrations, a decrease in the calcein fluorescence intensity was observed (data not shown). This might be due to self-quenching of the released calcein, and/or binding of the negatively charged calcein to the basic peptides (which also have a high propensity to aggregate) leading to formation of large peptide–calcein complexes, which results in further quenching of the calcein quantum yield. Such phenomena can distort the analysis.

With FCS, and the low concentrations of Rh required (in the nM range), this problem is mostly avoided. However, the affinity of Rh for phospholipids complicates the analysis (Table 3), suggesting the need for an alternative fluorophore. In addition, the presence of two forms of fluorescent particles with very different fluorescence intensities (in this case, Rh free in solution and Rh entrapped in the REVs) distort the quantitative evaluations [45].

The long N-terminal part of the PrP sequence is unstructured in aqueous solution [7]. The interaction of the signal peptide-containing domain with a membrane mediates secondary structure conversion towards β-sheet for the domain. Perhaps, this moiety can serve as a 'seed' for a structure conversion involving a larger part of the unprocessed PrP, possibly taking place at a membrane surface. A membrane-induced structure conversion in the N-terminus may also be important for the transformation from $PrP^{C}$ to $PrP^{Sc}$. The membrane-induced aggregation and structure conversion may be a common process for several amyloid forming proteins and peptides, as a general phenomenon leading to toxic effects in cellular systems (cf. [58,59]). Among the common amyloid proteins [58], only the unprocessed PrP has a hydrophobic signal sequence directly followed by a basic sequence, the combination of which is related to the CPP property of the N-terminal domain. This inherent property may facilitate intercellular prion trafficking, and furthermore contribute to the membrane perturbations, as observed in this study.

## Acknowledgements

We thank Mr. Torbjörn Astlind for expert technical assistance. This study was supported by grants from the Swedish Research Council and from the EU program contracts no. HPRN-CT-2001-00242; QLK3-CT-2002-01989.

## References

[1] S.B. Prusiner, Molecular biology of prion diseases, Science 252 (1991) 1515–1522.
[2] B. Caughey, P.T. Lansbury Jr., Protofibrils, pores, fibrils, and neurodegeneration: separating the responsible protein aggregates from the innocent bystanders, Annu. Rev. Neurosci. 26 (2003) 267–298.
[3] S.J. Collins, V.A. Lawson, C.L. Masters, Transmissible spongiform encephalopathies, Lancet 363 (2004) 51–61.
[4] N. Stahl, M.A. Baldwin, D.B. Teplow, L. Hood, B.W. Gibson, A.L. Burlingame, S.B. Prusiner, Structural studies of the scrapie prion protein using mass spectrometry and amino acid sequencing, Biochemistry 32 (1993) 1991–2002.
[5] D.A. Kocisko, J.H. Come, S.A. Priola, B. Chesebro, G.J. Raymond, P.T. Lansbury, B. Caughey, Cell-free formation of protease-resistant prion protein, Nature 370 (1994) 471–474.
[6] K.M. Pan, M.A. Baldwin, J. Nguyen, M. Gasset, A. Serban, D. Groth, I. Mehlhorn, Z. Huang, R.J. Fletterick, F.E. Cohen, S.B. Prusiner, Conversion of α-helices into β-sheets features in the formation of the scrapie prion proteins, Proc. Natl. Acad. Sci. U. S. A. 90 (1993) 10962–10966.
[7] F. Lopez Garcia, R. Zahn, R. Riek, K. Wüthrich, NMR structure of the bovine prion protein, Proc. Natl. Acad. Sci. U. S. A. 97 (2000) 8334–8339.
[8] R.S. Hegde, P. Tremblay, D. Groth, S.J. DeArmond, S.B. Prusiner, V.R. Lingappa, Transmissible and genetic prion diseases share a common pathway of neurodegeneration, Nature 402 (1999) 822–826.
[9] R.S. Hegde, J.A. Mastrianni, M.R. Scott, K.A. DeFea, P. Tremblay, M. Torchia, S.J. DeArmond, S.B. Prusiner, V.R. Lingappa, A transmembrane form of the prion protein in neurodegenerative disease, Science 279 (1998) 827–834.
[10] R.S. Stewart, D.A. Harris, Most pathogenic mutations do not alter the membrane topology of the prion protein, J. Biol. Chem. 276 (2001) 2212–2220.
[11] R.S. Stewart, D.A. Harris, A transmembrane form of the prion protein is localized in the Golgi apparatus of neurons, J. Biol. Chem. 280 (2005) 15855–15864.
[12] D.A. Harris, Trafficking, turnover and membrane topology of PrP, Br. Med. Bull. 66 (2003) 71–85.
[13] R.S. Stewart, B. Drisaldi, D.A. Harris, A transmembrane form of the prion protein contains an uncleaved signal peptide and is retained in the endoplasmic reticulum, Mol. Biol. Cell 12 (2001) 881–889.

[14] S.J. Kim, R. Rahbar, R.S. Hegde, Combinatorial control of prion protein biogenesis by the signal sequence and transmembrane domain, J. Biol. Chem. 276 (2001) 26132–26140.
[15] C.M. Ott, V.R. Lingappa, Signal sequences influence membrane integration of the prion protein, Biochemistry 43 (2004) 11973–11982.
[16] J. Ma, R. Wollmann, S. Lindquist, Neurotoxicity and neurodegeneration when PrP accumulates in the cytosol, Science 298 (2002) 1781–1785.
[17] B. Drisaldi, R.S. Stewart, C. Adles, L.R. Stewart, E. Quaglio, E. Biasini, L. Fioriti, R. Chiesa, D.A. Harris, Mutant PrP is delayed in its exit from the endoplasmic reticulum, but neither wild-type nor mutant PrP undergoes retrotranslocation prior to proteasomal degradation, J. Biol. Chem. 278 (2003) 21732–21743.
[18] L. Fioriti, S. Dossena, L.R. Stewart, R.S. Stewart, D.A. Harris, G. Forloni, R. Chiesa, Cytosolic prion protein (PrP) is not toxic in N2a cells and primary neurons expressing pathogenic PrP mutations, J. Biol. Chem. 280 (2005) 11320–11328.
[19] P. Lundberg, M. Magzoub, M. Lindberg, M. Hällbrink, J. Jarvet, L.E.G. Eriksson, Ü. Langel, A. Gräslund, Cell membrane translocation of the N-terminal (1–28) part of the prion protein, Biochem. Biophys. Res. Commun. 299 (2002) 85–90.
[20] H. Biverståhl, A. Andersson, A. Gräslund, L. Mäler, NMR solution structure and membrane interaction of the N-terminal sequence (1–30) of the bovine prion protein, Biochemistry 43 (2004) 14940–14947.
[21] Ü. Langel (Ed.), Cell Penetrating Peptides. Processes and Applications, CRC Press, Boca Raton, 2002.
[22] M. Magzoub, A. Gräslund, Cell-penetrating peptides: from inception to application, Q. Rev. Biophys. 37 (2004) 147–195.
[23] J.S. Wadia, R.V. Stan, S.F. Dowdy, Transducible TAT-HA fusogenic peptide enhances escape of TAT-fusion proteins after lipid raft macropinocytosis, Nat. Med. 10 (2004) 310–315.
[24] M. Belting, S. Sandgren, A. Wittrup, Nuclear delivery of macromolecules: barriers and carriers, Adv. Drug Deliv. Rev. 57 (2005) 505–527.
[25] O. Ben-Zaken, S. Tzaban, Y. Tal, L. Horonchik, J.D. Esko, I. Vlodavsky, A. Taraboulos, Cellular heparan sulfate participates in the metabolism of prions, J. Biol. Chem. 278 (2003) 40041–40049.
[26] N. Hijazi, Z. Kariv-Inbal, M. Gasset, R. Gabizon, PrPSc incorporation to cells requires endogenous glycosaminoglycan expression, J. Biol. Chem. 280 (2005) 17057–17061.
[27] M. Morillas, W. Swietnicki, P. Gambetti, W.K. Surewicz, Membrane environment alters the conformational structure of the recombinant human prion protein, J. Biol. Chem. 274 (1999) 36859–36865.
[28] P. Critchley, J. Katzlauskaite, R. Eason, T. Pinheiro, Binding of prion proteins to lipid membranes, Biochem. Biophys. Res. Commun. 313 (2004) 559–567.
[29] A. Pramanik, J. Widengren, Fluorescence correlation spectroscopy (FCS), in: R.A. Meyers (Ed.), Encyclopedia of Molecular Cell Biology and Molecular Medicine, Willey-VCH, 2004, pp. 461–500.
[30] J.R. Lakowicz, Principles of Fluorescence Spectroscopy, 2nd ed., Kluwer Academic, New York, 1999.
[31] R. Rigler, Ü. Mets, Diffusion of single molecules through a Gaussian laser beam, Soc. Photo-Opt. Instrum. Eng. 1921 (1993) 239–248.
[32] R. Rigler, J. Widengren, Ü. Mets, in: O.J. Wolfbeis (Ed.), Fluorescence Correlation Spectroscopy, Springer Verlag, Berlin, 1992.
[33] M. Ehrenberg, R. Rigler, Rotational Brownian motion and fluorescence intensity fluctuation, Chem. Phys. 4 (1974) 390–401.
[34] E.L. Elson, D. Magde, Fluorescence correlation spectroscopy: I. Conceptual basis and theory, Biopolymers 13 (1974) 1–27.
[35] R. Rigler, Ü. Mets, J. Widengren, P. Kask, Fluorescence correlation spectroscopy with high count rate and low background: analysis of translational diffusion, Eur. Biophys. J. 22 (1993) 169–175.
[36] D.W. Marquardt, An algorithm for least-squares estimates of nonlinear parameters, J. Soc. Ind. Appl. Math. 11 (1963) 431–441.
[37] P. Manavalan, W.C. Johnson Jr., Variable selection method improves the prediction of protein secondary structure from circular dichroism spectra, Anal. Biochem. 167 (1987) 76–85.
[38] K. Matsuzaki, S. Yoneyama, K. Miyajima, Pore-formation and translocation of melittin, Biophys. J. 73 (1997) 831–838.
[39] M. Magzoub, K. Kilk, L.E.G. Eriksson, Ü. Langel, A. Gräslund, Comparison of the interaction, positioning, structure induction and membrane perturbation of cell-penetrating peptides and non-translocating variants with phospholipid vesicles, Biochim. Biophys. Acta 1516 (2001) 77–89.
[40] M. Magzoub, L.E.G. Eriksson, A. Gräslund, Interaction and structure induction of cell-penetrating peptides in the presence of phospholipid vesicles, Biophys. Chem. 103 (2003) 271–288.
[41] B.R. Lentz, Use of fluorescent probes to monitor molecular order and motions within liposome bilayers, Chem. Phys. Lipids 64 (1993) 99–110.
[42] J. Repakova, J.M. Holopainen, M.R. Morrow, M.C. McDonald, P. Capkova, L. Vattulainen, Influence of DPH on the structure and dynamics of a DPPC bilayer, Biophys J. 88 (2005) 3398–3410.
[43] W.C. Wimley, S.H. White, Determining the membrane topology of peptides by fluorescence quenching, Biochemistry 39 (2000) 161–170.
[44] M. Lindberg, H. Biverståhl, A. Gräslund, L. Mäler, Structure and positioning comparison of two variants of penetratin in two different membrane mimicking systems by NMR, Eur. J. Biochem. 270 (2004) 3055–3063.
[45] J.D. Müller, Y. Chen, E. Gratton, Resolving heterogeneity on the single molecular level with the photon-counting histogram, Biophys. J. 78 (2000) 474–486.
[46] A. Pramanik, P. Thyberg, R. Rigler, Molecular interactions of peptides with phospholipids vesicle membranes as studied by fluorescence correlation spectroscopy, Chem. Phys. Lipids 104 (2000) 35–47.
[47] A. Pramanik, Molecular interaction of peptides with phospholipid membranes by fluorescence correlation spectroscopy (FCS), Recent Res. Dev. Chem. Phys. Lipids 1 (2003) 53–70.
[48] M. Magzoub, L.E.G. Eriksson, A. Gräslund, Conformational states of the cell-penetrating peptide penetratin when interacting with phospholipid vesicles: effects of surface charge and peptide concentration, Biochim. Biophys. Acta 1563 (2002) 53–63.
[49] P.E.G. Thorén, D. Persson, P. Isakson, M. Goksör, A. Önfelt, B. Nordén, Uptake of analogs of penetratin, Tat(48–60) and oligoarginine in live cells, Biochem. Biophys. Res. Commun. 307 (2003) 100–107.
[50] T. Benachir, M. Lafleur, Study of vesicle leakage induced by melittin, Biochim. Biophys. Acta 1235 (1995) 452–460.
[51] K. Takeshima, A. Chikushi, K.-K. Lee, S. Yonehara, K. Matsuzaki, Translocation of analogues of the antimicrobial peptides magainin and buforin across human cell membranes, J. Biol. Chem. 278 (2003) 1310–1315.
[52] M.T. Lee, F.Y. Chen, H.W. Huang, Energetics of pore formation induced by membrane active peptides, Biochemistry 43 (2004) 3590–3599.
[53] M. Matsuzaki, K. Yasuyuki, O. Akada, S. Murase, M. Yoneyama, K. Zasloff, Mechanism of synergism between antimicrobial peptides magainin 2 and PGLa, Biochemistry 37 (1998) 15144–15153.
[54] L. Zhang, A. Rozek, R.E.W. Hancock, Interaction of cationic antimicrobial peptides with model membranes, J. Biol. Chem. 276 (2001) 35714–35722.
[55] D. Oh, S.Y. Shin, S. Lee, J.H. Kang, S.D. Kim, P.D. Ryu, K.-S. Hahm, Y. Kim, Role of the hinge region and the tryptophan residue in the synthetic antimicrobial peptides, cecropin A(1–8)–magainin 2(1–12) and its analogues, on their antibiotic activities and structures, Biochemistry 39 (2000) 11855–11864.
[56] A. Arbuzova, G. Schwarz, Pore-forming action of mastoparan peptides on liposomes: a quantitative analysis, Biochim. Biophys. Acta 1420 (1999) 139–152.
[57] R.F. Chen, J.R. Knutson, Mechanism of fluorescence concentration quenching of carboxyfluorescein in liposomes: energy transfer to nonfluorescent dimmers, Anal. Biochem. 172 (1988) 61–77.
[58] M. Stefani, C.M. Dobson, Protein aggregation and aggregate toxicity: new insights into protein folding, misfolding diseases and biological evolution, J. Mol. Med. 81 (2003) 678–699.
[59] A. Quist, I. Duodevski, H. Lin, R. Azimova, D. Ng, B. Frangione, B. Kagan, J. Ghiso, R. Lal, Amyloid ion channels: a common structural link for protein-misfolding disease, Proc. Natl. Acad. Sci. U. S. A. 102 (2005) 10427–10432.
[60] J. Kyte, R.F. Doolittle, A simple method for displaying the hydropathic character of a protein, J. Mol. Biol. 157 (1982) 105–132.